

RESEARCH ARTICLE | NOVEMBER 24 2025

On the role of high speed electron beams in the generation of subsonic solitons on electron dynamic timescales

S. K. Maharaj ; R. Bharuthram 



Phys. Plasmas 32, 112303 (2025)

<https://doi.org/10.1063/5.0274881>



Articles You May Be Interested In

The role of ion beams in the propagation of linear and nonlinear ion-acoustic waves in space plasmas

Phys. Plasmas (August 2025)

Arbitrary amplitude fast electron-acoustic solitons in three-electron component space plasmas

Phys. Plasmas (June 2016)

Coupling between nonlinear Alfvén waves and reduced magnetohydrodynamics for compressible fluids

Phys. Plasmas (August 1999)



Physics of Plasmas

Special Topics Open
for Submissions

[Learn More](#)

On the role of high speed electron beams in the generation of subsonic solitons on electron dynamic timescales

Cite as: Phys. Plasmas **32**, 112303 (2025); doi: 10.1063/5.0274881

Submitted: 9 April 2025 · Accepted: 1 November 2025 ·

Published Online: 24 November 2025



View Online



Export Citation



CrossMark

S. K. Maharaj^{1,a)}  and R. Bharuthram^{2,b)} 

AFFILIATIONS

¹South African National Space Agency (SANSA) Space Science, P. O. Box 32, Hermanus 7200, South Africa

²Department of Physics and Astronomy, University of the Western Cape, Robert Sobukwe Road, Bellville 7535, South Africa

^{a)} Author to whom correspondence should be addressed: smaharaj@sansa.org.za

^{b)} Electronic mail: rbharuthram@uwc.ac.za

ABSTRACT

A comprehensive theoretical investigation of the effects of electron beams on high frequency electron-acoustic waves is conducted for plasmas comprising two warm (adiabatic) electron components, Boltzmann electrons, and immobile ions of which one or both adiabatic electron fluid components are modeled as drifting (beams). A systematic approach is followed, starting with a single beam model comprising cool electrons, warm beam electrons, and hot electrons consistent with Berthomier *et al.* [Phys. Plasmas **7**, 2987–2994 (2000)] and then proceeding to models with asymmetric and symmetric counterstreaming electron beams. The subsonic character of the solitons in the nonlinear regime is attributed to the effect of the beam(s) that support(s) the directional change of the backward propagating fast (or both slow mode) waves in the model with a single (counterstreaming) beam(s). This results in the coupling of two wave modes, which decouple for higher beam speeds. The results of our study are generic to other plasma systems containing heavier inertial plasma components as the findings are very similar to ion beam effects on low frequency ion-acoustic waves reported by Zank and McKenzie [J. Plasma Phys. **39**, 183–191 (1988)] and Lakhina *et al.* [Phys. Scr. **95**, 105601 (2020)] in models with a single and counterstreaming ion beams, respectively. In fact, similar reasoning applies in validating the generation of subsonic waves in the above reports as it relates to the directional change(s) of the linear wave(s), which also explains the generation of subsonic waves in the paper by Berthomier and coworkers in a single beam model.

© 2025 Author(s). All article content, except where otherwise noted, is licensed under a Creative Commons Attribution-NonCommercial 4.0 International (CC BY-NC) license (<https://creativecommons.org/licenses/by-nc/4.0/>). <https://doi.org/10.1063/5.0274881>

I. INTRODUCTION

The electron-acoustic mode is a fundamental high frequency electrostatic wave that propagates in a plasma with two-temperature (cool and hot) electrons. The propagation of this wave, which relies on inertial effects of the cool electrons and restoring force provided by the pressure of the hot electrons, is the high frequency analog of the ion-acoustic wave.

The electron-acoustic mode has been theoretically investigated by several authors in both the linear and nonlinear wave regimes. The relative streaming between the cool and hot electrons or between one or more electron components in models with more than two electron species excites the electron-acoustic or electron streaming instabilities, which have been investigated by several authors in plasmas with a single^{1–3} or counterstreaming^{1,4,5} electron beams.

In the nonlinear regime, the electron-acoustic mode propagates as solitons, which are propagating bell-shaped pulses in potential. The nonlinear propagation characteristics of the electron-acoustic wave were investigated in an early study by Mace *et al.*⁶ in a model with cool inertial electrons, hot Boltzmann electrons, and inertial ions. The supported solitons were found to have negative polarity.

The modeling in the theoretical studies especially as relates to electron-acoustic waves has been motivated by several satellite observations including FAST in the downward current region of the mid-altitude auroral region,⁷ Polar satellite in the high altitude polar magnetosphere,⁸ Geotail in the magnetotail,⁹ Wind¹⁰ in the terrestrial bow shock and CLUSTER in the dayside magnetosheath,¹¹ of electrostatic solitary waves with bipolar shaped electric field waveforms which are parallel to the magnetic field. The formation of the observed

structures, which are reliant on electron dynamics, are found to have positive potential signatures. The positive polarity structures are interpreted¹² as “electron holes” which appear as BGK solutions involving trapped and untrapped electron populations in a Vlasov–Poisson system of equations or as electrostatic solitary waves.

In attempting to offer a theoretical explanation for the observed nonlinear structures, the extension of the theoretical model with inertial cool electrons and inertialess hot electrons to include an electron beam by Berthomier *et al.*¹³ appears to have been a step in the right direction in interpreting the observations, noting that the nonlinear structures that are supported in the model of Ref. 6 are contradictory to the observations as the model predicts only negative polarity structures can occur. Nevertheless, the generation of positive polarity solitons has been shown to occur in a simpler model by Cattaert *et al.*¹⁴ with the incorporation of inertial effects but not including streaming for the hot electrons. Similar reasoning applies in explaining the occurrence of electron-acoustic (or slow electron solitons), which have positive polarity reported by Maharaj *et al.*¹⁵ (or Singh *et al.*¹⁶ and Mbuli *et al.*¹⁷), which is reliant on retaining inertial effects of the hot (or warm electrons) in plasma models with two¹⁵ (or three^{16,17}) electron components. The existence of slow and fast electron-acoustic solitons associated with the slow¹⁷ and fast¹⁸ electron-acoustic modes is supported in plasmas containing three electron constituents, of which at least two are inertial fluid components. The distinction between the cool, warm, and hot electrons in the investigated models is a result of the disparity between the thermal speeds of the constituent electrons.

A similar phenomenon arises in a theoretical model with two inertial plasma constituents, which is driven primarily by high speed beam effects and not by differences in the thermal speeds of the inertial beam plasma components. This invokes the existence of a class of “slow” solitons in plasmas with sufficiently high speed beam components. This has been investigated more recently by Lakhina *et al.*¹⁹ in which solitons associated with the ion-acoustic mode, which propagate for speeds below the critical acoustic speeds of the linear waves, have been reported to occur in a plasma with symmetric counterstreaming ion beams. It has been confirmed in a subsequent study by Verheest and Hellberg²⁰ based on a simpler model to that in Ref. 19, but one which neglects thermal effects of the counterstreaming beams, that these solitons are indeed subsonic (propagate for speeds that are below the acoustic speed). The supported nonlinear structures have amplitudes that diminish with increasing soliton speed and vanish at the acoustic speed as observed from a (stationary) laboratory frame.

To the best of our knowledge, the paper by Zank and McKenzie²¹ appears to be the very first report on the occurrence of subsonic ion-acoustic solitons generated by high speed beams, however in a model with a single ion beam in contrast to the models with counterstreaming ion beams in Refs. 19 and 20. In a similar vein, it appears that Berthomier *et al.*¹³ were the first to report on the occurrence of subsonic solitons on the short timescale of electron dynamics synonymous with the high frequency electron-acoustic wave in a plasma with non-drifting cool electrons, a warm electron beam, and Boltzmann hot electrons. The main thrust of their investigation is on the role of the warm electron beam in supporting the existence of electron-acoustic solitons having positive polarity. More recent investigations include the study by Singh *et al.*²² in which subsonic ion-acoustic waves are discussed in a model with counterstreaming ion beams (symmetric and

asymmetric) and kappa-distributed electrons. The latest report on the topic of subsonic waves generated by high speed beams is the study by Maxengana *et al.*²³ of subsonic ion-acoustic waves, which have been investigated for plasma models with a single and counterstreaming ion beams.

Our main interest in this paper is on the role of electron beams in the generation of slow waves which are subsonic in the high frequency regime. We consider the generation of subsonic waves by high speed beams to be a novel area of research as the focus in the earlier^{16–18} studies was on slow and fast waves that arise due to differences in thermal speeds of the constituent electrons, for which beams are not needed. In fact, the novelty of the research on subsonic waves generated by high speed beams has also been attested to in the more recent study by Singh *et al.*,²² who also point out that the bulk of the theoretical investigations until now has mainly been on solitary waves that are supersonic in a very wide variety of plasma models. The generation of the slow waves in the context of our study, which is reliant on the presence of high speed beams is consistent with the earlier studies in Refs. 19–22 in which subsonic waves are investigated in models with ion beams. It is necessary to point out that the focus in the earlier studies was more on the features but not on the actual generation mechanism of the subsonic waves, which is our primary undertaking here. This has been addressed most recently in the study by Maxengana *et al.* in Ref. 23, and is attributed to the directional changes of the linear waves under the influence of the ion beams in the respective models with a single and counterstreaming ion beams, which are asymmetric and symmetric.

We redirect our efforts to show here that a similar phenomenon occurs in the high frequency regime, as it relates to the effects of electron beams in the generation of high frequency waves, which are subsonic. In doing so, we follow a systematic approach by investigating first the model with a single electron beam and proceed next to the model with asymmetric and then symmetric counterstreaming electron beams in this order. The reason for this ordering is that the results in the single beam model aid in the interpretation of the results in the second model with asymmetric electron beams, which, in turn, provides insights into understanding the effects of symmetric counterstreaming beams in the third model. The detailed linear analyses in terms of the effect of beam speed on the plots of $\omega(k)$, which we include as a prequel to the nonlinear studies for all three models, is vital for the understanding of how the subsonic character of the waves in the nonlinear regime arises, which insights are missing in Refs. 13, 19, 20, 21, and 22. The results of our study are relevant for a variety of plasma environments within the terrestrial magnetosphere, including the day-side polar cusp²⁴ and auroral²⁵ regions where single electron beams occur, and separatrix²⁶ regions of magnetic reconnection sites where counterstreaming electron beams occur.

Following this introduction, we present details of the theory in Sec. II which is subdivided into Secs. II A and II B that discuss aspects of the theory related to linear and nonlinear waves, respectively. The results in the model with non-drifting cool electrons, hot electrons, and a single warm electron beam are discussed in Sec. III. The results in the model with asymmetric counterstreaming electron beams, which are cool and warm, are presented in Sec. IV. This is followed by the model with symmetric counterstreaming beams in Sec. V. For each model in Secs. III–V, the results in the linear and nonlinear regimes

are discussed in Secs. III A, III B, IV A, IV B, V A, and V B, respectively. To conclude, a summary of our findings is presented in Sec. VI.

II. THEORY

We initially consider a general four-component plasma model with two (counterstreaming) electron beams, Boltzmann hot electrons and immobile ions. The set of governing equations for such a general model can be reduced to special situations corresponding to a single electron beam, asymmetric and symmetric counterstreaming electron beams by an appropriate choice of electron densities, temperatures and beam speeds as will be seen in the next three sections.

The ions are modeled as immobile and provide a neutralizing background, which is justified on short timescale fluctuation phenomena associated with electron dynamics. The ion density remains fixed at its equilibrium value satisfying $N_i = N_{i0} = \text{const}$.

We assume a Boltzmann distribution for the hot electrons with number density in normalized form given by

$$N_h = \exp(\Phi), \quad (1)$$

where Φ is the normalized electrostatic potential.

The dynamics of the two counterstreaming electron beam plasma components are governed by the set of fluid equations¹⁶ given by

$$\frac{\partial N_j}{\partial t} + \frac{\partial}{\partial x}(N_j V_j) = 0, \quad (2)$$

$$\frac{\partial V_j}{\partial t} + V_j \frac{\partial V_j}{\partial x} = \frac{\partial \Phi}{\partial x} - \frac{1}{N_j} \frac{\partial P_j}{\partial x}, \quad (3)$$

$$\frac{\partial P_j}{\partial t} + V_j \frac{\partial P_j}{\partial x} + 3P_j \frac{\partial V_j}{\partial x} = 0. \quad (4)$$

The system of equations is closed by Poisson's equation

$$\frac{\partial^2 \Phi}{\partial x^2} = \sum_j N_j + N_h - N_i. \quad (5)$$

Here N_j , V_j , P_j , respectively, are the number density, velocity and pressure of the different electron beam species j and Φ is the electrostatic potential. We have used the adiabatic equation of state (4) with polytropic index $\gamma = 3$ for the cool and warm beam electrons. The densities are normalized by the total electron density $n_0 = n_{j0} = n_{bv0} + n_{bc0} + n_{h0}$, velocities by the thermal speed of the hot electrons $v_{the} = (k_B T_h / m_e)^{1/2}$, lengths by $\lambda_{de} = (\epsilon_0 k_B T_h / n_0 e^2)^{1/2}$, time by the inverse electron plasma frequency $\omega_{pe}^{-1} = (n_0 e^2 / \epsilon_0 m_e)^{-1/2}$, temperature by hot electron temperature T_h , potential by $k_B T_h / e$ and pressure by $n_0 T_h$.

A. Linear analysis

The dimensional forms of the set of Eqs. (2)–(5), including Eq. (1), are linearized, which yields the linear wave dispersion relation

$$\sum_j \frac{\omega_{pj}^2}{(\omega - kv_{j0})^2 - 3k^2 v_{ij}^2} - \frac{1}{k^2 \lambda_{dhe}^2} - 1 = 0, \quad (6)$$

where the plasma frequency $\omega_{pj} = (n_{j0} e^2 / \epsilon_0 m_e)^{1/2}$, thermal speed $v_{ij} = (k_B T_j / m_e)^{1/2}$ and Debye shielding length $\lambda_{dhe} = (\epsilon_0 k_B T_h / n_{h0} e^2)^{1/2}$. Here, the v_{j0} denote the dimensional speeds of the electron beam components at equilibrium.

Normalizing frequencies with respect to the inverse total electron plasma frequency $\omega_{pe}^{-1} = (n_0 e^2 / \epsilon_0 m_e)^{-1/2}$, thermal speeds by the hot electron thermal speed $v_{the} = (k_B T_h / m_e)^{1/2}$ and lengths by $\lambda_{de} = (\epsilon_0 k_B T_h / n_0 e^2)^{1/2}$, we obtain the dimensionless form of the dispersion relation (6) given by

$$\sum_j \frac{N_{j0}}{(\Omega - KV_{j0})^2 - 3K^2 \sigma_j} - \frac{N_{h0}}{K^2} - 1 = 0, \quad (7)$$

which, after multiplying by K^2 , can be written in the form

$$\sum_j \frac{N_{j0}}{(M - V_{j0})^2 - 3\sigma_j} - N_{h0} - K^2 = 0, \quad (8)$$

where the dimensionless wave phase speed $M = \Omega / K$ is a ratio of the dimensionless frequency Ω and wavenumber K . Here $V_{j0} (\equiv v_{j0} / v_{the})$, $N_{j0} (\equiv n_{j0} / n_0)$ and $\sigma_j (\equiv T_j / T_h)$ are now dimensionless quantities denoting the speed, density, and temperature of the electron beams.

The dispersion relation (7) can be rewritten as

$$\frac{N_{b10}}{(\Omega - KV_{b10})^2 - 3K^2 \sigma_{b1}} + \frac{N_{b20}}{(\Omega - KV_{b20})^2 - 3K^2 \sigma_{b2}} - \frac{N_{h0}}{K^2} - 1 = 0. \quad (9)$$

B. Nonlinear study

In order to study the properties of the nonlinear structures of arbitrary amplitudes, we transform the set of Eqs. (2)–(5) to the stationary frame $\zeta = x - Mt$ where $M = V / v_{the}$ is the normalized solitary wave speed with respect to the hot electron thermal speed.

We obtain expressions for the densities by integrating Eqs. (2)–(4), making use of the following boundary conditions for localized solutions

$$N_h \rightarrow N_{h0}, \quad N_j \rightarrow N_{j0}, \quad V_j \rightarrow V_{j0}, \quad P_j \rightarrow N_{j0} \sigma_j, \\ \Phi \rightarrow 0 \quad \text{and} \quad \frac{d\Phi}{d\zeta} \rightarrow 0 \quad \text{as} \quad |\zeta| \rightarrow \pm\infty. \quad (10)$$

We follow popular practice in rewriting the obtained expressions for the densities in the form proposed by Ghosh *et al.*²⁷ for ease of integration of Poisson's equation in obtaining the expression for the Sagdeev pseudopotential. This density expression is signed [for an example, cf. Eq. (11) in Ref. 28] such that the solution, which coincides with the plus and minus sign, corresponds to subsonic and supersonic species, respectively. When substituted into Poisson's equation, this yields a signed expression for the Sagdeev pseudopotential [for an example, cf. Eq. (15) in Ref. 28] after integration.

In order to eliminate the inconvenience of using a signed version of the Sagdeev pseudopotential for which different expressions apply for solutions for solitons associated with the fast and slow mode waves, we follow the ideas in Olivier *et al.*²⁹ in using a "factored" form for the density expressions for the beam electrons in our model which is given by

$$N_j = \frac{N_{j0} [(M - V_{j0}) + \sqrt{3\sigma_j}]}{2\sqrt{3\sigma_j}} \left(1 + \frac{2\Phi}{[(M - V_{j0}) + \sqrt{3\sigma_j}]^2} \right)^{1/2} - \frac{N_{j0} [(M - V_{j0}) - \sqrt{3\sigma_j}]}{2\sqrt{3\sigma_j}} \left(1 + \frac{2\Phi}{[(M - V_{j0}) - \sqrt{3\sigma_j}]^2} \right)^{1/2}. \tag{11}$$

The solution corresponding to the upper sign (“+”) in front of the second term was discarded from Eq. (11) as the solution corresponding to the lower sign (“−”) applies to both supersonic and

subsonic species [satisfying $N_j \rightarrow N_{j0}$ in accordance with Eq. (10)] as pointed out in Ref. 29 which refers the reader to the Appendix in Ref. 30.

The expressions (1) for the Boltzmann hot electrons and Eq. (11) for the electron beam fluid components are then substituted in Poisson’s equation (5).

Integrating Poisson’s equation, we obtain the energy integral

$$\frac{1}{2} \left(\frac{d\Phi}{d\zeta} \right)^2 + V(\Phi, M) = 0, \tag{12}$$

where the Sagdeev pseudopotential is given by

$$V(\Phi, M) = N_{h0}(1 - e^\Phi) + N_{i0}\Phi + \sum_j \frac{N_{j0}((M - V_{j0}) + \sqrt{3\sigma_j})^3}{6\sqrt{3\sigma_j}} \left\{ 1 - \left(\sqrt{1 + \frac{2\Phi}{((M - V_{j0}) + \sqrt{3\sigma_j})^2}} \right)^3 \right\} - \sum_j \frac{N_{j0}((M - V_{j0}) - \sqrt{3\sigma_j})^3}{6\sqrt{3\sigma_j}} \left\{ 1 - \left(\sqrt{1 + \frac{2\Phi}{((M - V_{j0}) - \sqrt{3\sigma_j})^2}} \right)^3 \right\}. \tag{13}$$

This unsigned expression for the Sagdeev pseudopotential (13) will yield solutions for solitons for both the slow and fast electron-acoustic modes in the present form precisely as written.

The expression (13) can be rewritten in the form

$$V(\Phi, M) = N_{h0}(1 - e^\Phi) + N_{i0}\Phi + \frac{N_{b10}((M - V_{b10}) + \sqrt{3\sigma_{b1}})^3}{6\sqrt{3\sigma_{b1}}} \left\{ 1 - \left(\sqrt{1 + \frac{2\Phi}{((M - V_{b10}) + \sqrt{3\sigma_{b1}})^2}} \right)^3 \right\} - \frac{N_{b10}((M - V_{b10}) - \sqrt{3\sigma_{b1}})^3}{6\sqrt{3\sigma_{b1}}} \left\{ 1 - \left(\sqrt{1 + \frac{2\Phi}{((M - V_{b10}) - \sqrt{3\sigma_{b1}})^2}} \right)^3 \right\} + \frac{N_{b20}((M - V_{b20}) + \sqrt{3\sigma_{b2}})^3}{6\sqrt{3\sigma_{b2}}} \left\{ 1 - \left(\sqrt{1 + \frac{2\Phi}{((M - V_{b20}) + \sqrt{3\sigma_{b2}})^2}} \right)^3 \right\} - \frac{N_{b20}((M - V_{b20}) - \sqrt{3\sigma_{b2}})^3}{6\sqrt{3\sigma_{b2}}} \left\{ 1 - \left(\sqrt{1 + \frac{2\Phi}{((M - V_{b20}) - \sqrt{3\sigma_{b2}})^2}} \right)^3 \right\}. \tag{14}$$

1. Existence criteria for solitons

In proceeding to investigate beam effects on solitons in the non-linear regime, we include here the expressions for the second and third derivatives of the Sagdeev pseudopotential (13).

The requirement for the existence of soliton solutions is that the second derivative of the expression for the Sagdeev pseudopotential, i.e., $F(M) = V''(\Phi, M)$ which evaluated at $\Phi = 0$, must satisfy

$$F(M) = \sum_j \frac{N_{j0}}{(M - V_{j0})^2 - 3\sigma_j} - N_{h0} \leq 0. \quad (15)$$

This condition establishes lower limits for M (M_{\min}) for the existence of solitons, which must satisfy $F(M) = 0$, i.e.,

$$F(M) = \sum_j \frac{N_{j0}}{(M_{\min} - V_{j0})^2 - 3\sigma_j} - N_{h0} = 0, \quad (16)$$

which becomes

$$F(M) = \frac{N_{b10}}{(M - V_{b10})^2 - 3\sigma_{b1}} + \frac{N_{b20}}{(M - V_{b20})^2 - 3\sigma_{b2}} - N_{h0} = 0. \quad (17)$$

We refer to the M_{\min} values satisfying $F(M) = 0$ as the critical acoustic speeds which have to be exceeded for the existence of solitons.

On the other hand, the upper limit on M for soliton existence as it applies to the negative polarity structures coincides with the value of M_{\max} , which, if exceeded, the density of one of the inertial electron beam components given by Eq. (11) becomes complex valued. This establishes the existence of an upper limit on the amplitude Φ_{\max} of the supported negative potential solitons, which must satisfy

$$\Phi \leq \Phi_{\max,j} = -\left[(M - V_{j0}) - \sqrt{3\sigma_j}\right]^2 / 2.$$

The density will break down at the lower of the two upper potentials such that the soliton amplitudes cannot exceed $\min\{\Phi_{\max,bc}, \Phi_{\max,bw}\}$ using the example of the model with cool beam ($j = bc$) and warm beam electrons ($j = bw$) which is discussed in Sec. IV to elaborate on this point. This limits the admissible M range of the supported solitons to $M_{\min} < M < M_{\max}$ where $M_{\max} = \min\{M_{\max,bc}, M_{\max,bw}\}$. Similar arguments apply to the two upper potentials in the models with a single warm electron beam and non-drifting cool electrons ($j = bw, c$) (Sec. III) and symmetric counterstreaming electron beams ($j = b1, b2$) (Sec. V). The two upper potentials will have the same magnitude in the symmetric beam model.

Since in our model the ions are stationary, there is no density expression associated with dynamic ions to limit the existence of positive polarity solitons, which have been shown to be limited by the occurrence of a double layer in Ref. 14.

We have additionally included here the expression for the third derivative of the Sagdeev pseudopotential $V'''(\Phi, M)$ evaluated at $\Phi = 0$, yielding

$$G(M) = \sum_j -\frac{3N_{j0}(\sigma_j + (M - V_{j0})^2)}{(-3\sigma_j + (M - V_{j0})^2)^3} - N_{h0}, \quad (18)$$

which can be used to determine the polarity of the solitons which have a sech^2 profile in the limit of small wave amplitude as guided by the expression (28) in the study by Berthomier *et al.*¹³

III. MODEL WITH A SINGLE ELECTRON BEAM

A. Linear results

We start with the model consisting of a beam of warm electrons ($j = bw$), non-drifting cool ($j = c$) and hot electrons. The dispersion relation in this model given by

$$\frac{N_{c0}}{\Omega^2 - 3K^2\sigma_c} + \frac{N_{bw0}}{(\Omega - KV_{bw0})^2 - 3K^2\sigma_{bw}} - \frac{N_{h0}}{K^2} - 1 = 0, \quad (19)$$

was obtained from the dispersion relation for a plasma with counterstreaming beams [Eq. (9)], by replacing the subscripts “b1” and “b2” with “bw” and “c,” respectively, and setting $V_{bc0} = 0$. The fixed parameters are $N_{c0} = 0.4$, $N_{bw0} = 0.2$, $\sigma_c = 0.001$, and $\sigma_{bw} = 0.2$ for the densities and temperatures of the cool and warm beam electrons, respectively, and $N_{h0} = 0.4$ is the density of the hot electrons. The numerical solutions of Eq. (19) for the dimensionless complex frequency ω/ω_{pe} ($\equiv \Omega$) having real and imaginary parts ω_r/ω_{pe} ($\equiv \Omega_r$) and γ/ω_{pe} ($\equiv \Omega_i$) as a function of the dimensionless wavenumber $k\lambda_{de}$ ($\equiv K$) for the various supported waves are depicted in Fig. 1 for different values of the speed of the warm electron beam.

The dispersion curves when beam effects of the warm electrons are not included ($V_{bw0} = 0$) are shown in panel (a) in Fig. 1. There are two fast electron-acoustic modes, one with $\omega_r/\omega_{pe} > 0$ and the other with $\omega_r/\omega_{pe} < 0$ denoted by the red and orange curves, respectively. There are also two slow electron-acoustic modes of which one has $\omega_r/\omega_{pe} > 0$ and the other $\omega_r/\omega_{pe} < 0$ denoted by the blue and green curves, respectively. We refer to the two directions in which the slow and fast waves with positive ($(\omega_r/\omega_{pe})/k\lambda_{de} > 0$) and negative phase velocities ($(\omega_r/\omega_{pe})/k\lambda_{de} < 0$) propagate as the forward (to the right) and backward directions (to the left), respectively.

The dispersion curves for a higher $V_{bw0} = 0.8$ in panel (b) demonstrates an interesting effect in that the fast mode (orange) that was propagating in the backward direction for $V_{bw0} = 0$ [panel (a)] changes direction and propagates in the forward direction for $V_{bw0} = 0.8$ [panel (b)].

For an even higher $V_{bw0} = 1.0$ (panel (c)) the fast mode (orange) that has changed direction, couples with the slow mode that is propagating in the forward direction (blue). The result of this coupling is that the dispersion curve corresponding to ω_r/ω_{pe} is double-branched in frequency over regions of small $k\lambda_{de}$ (< 1.569) and large $k\lambda_{de}$ (> 3.895). The plasma also becomes unstable to the beam instability as the frequencies ω/ω_{pe} of the two modes, which have coupled become complex valued, one with a positive valued imaginary part ($\gamma/\omega_{pe} > 0$) (magenta) and the other with a negative valued imaginary part ($\gamma/\omega_{pe} < 0$) (brown) signifying damping. This growth/damping occurs over an intermediate region in $k\lambda_{de}$ ($1.569 \leq k\lambda_{de} \leq 3.895$) where the dispersion curve corresponding to ω_r/ω_{pe} is single-branched over $k\lambda_{de}$ (cyan colored portion of curve).

We observe here that the fast mode which was propagating in the backward direction (orange) and changed propagation direction to the forward direction and coupled with the forward propagating slow mode (blue), has not yet completely overtaken the forward propagating slow mode as the orange portion of the curve is still below the blue curve in the region of small $k\lambda_{de}$ (< 1.569). However, the behavior is different for large $k\lambda_{de}$ (> 3.895) where we observe that the orange portion of the curve is above the blue curve. The cyan colored portion of the dispersion curve for intermediate $k\lambda_{de}$ ($1.569 \leq k\lambda_{de} \leq 3.895$) where growth/damping occurs is common to both modes.

It becomes evident that the two coupled modes start to decouple for a higher $V_{bw0} = 1.2$ [panel (d)]. This is evident from the dispersion curve for ω_r/ω_{pe} which is no longer double-branched in the region of small $k\lambda_{de}$ and the regime for instability/damping shifts now to the

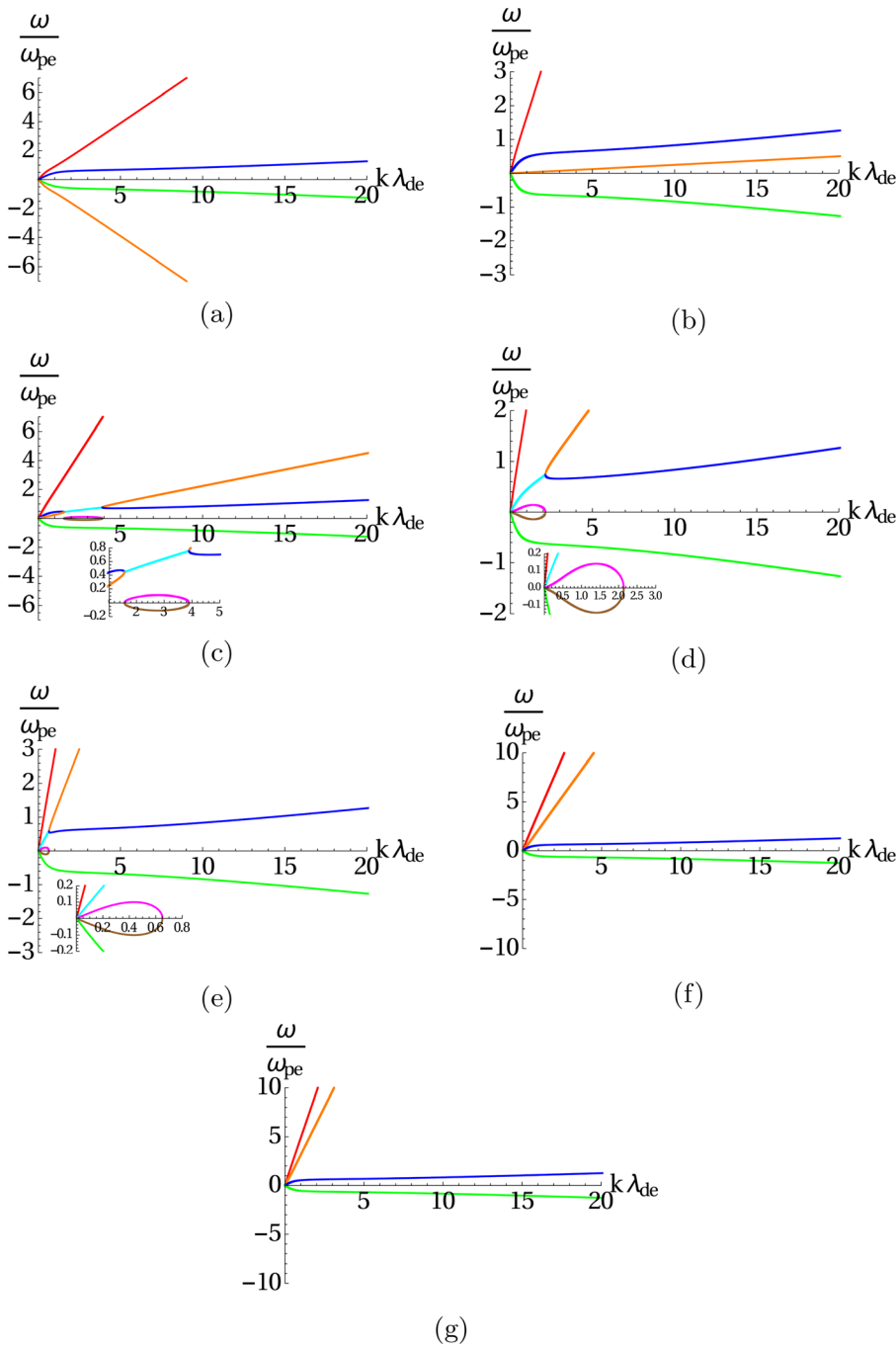


FIG. 1. Dispersion curves for the real frequency ω_r/ω_{pe} (red, blue, orange, green, cyan) and growth (magenta) and damping rate (brown) γ/ω_{pe} for (a) $V_{bw0} = 0$, (b) $V_{bw0} = 0.8$, (c) $V_{bw0} = 1.0$, (d) $V_{bw0} = 1.2$, (e) $V_{bw0} = 2$, (f) $V_{bw0} = 3$, and (g) $V_{bw0} = 4$. The insets provide magnified views of the regions of instability and damping. The fixed parameters are $\sigma_c = 0.001$, $\sigma_{bw} = 0.2$, $N_{r0} = 0.4$, $N_{c0} = 0.4$, and $N_{bw0} = 0.2$.

region of small $k\lambda_{de}$. The region in $k\lambda_{de}$ where instability/damping occurs diminishes for a higher $V_{bw0} = 2$ [panel (e)] which signifies further decoupling of the two modes.

We observe that the two modes are uncoupled for the higher $V_{bw0} = 3$ [panel (f)] and $V_{bw0} = 4$ [panel (g)]. This is evident from the dispersion curves for ω_r/ω_{pe} for the two modes (orange and blue) which have separated and are now distinct.

The effect of symmetry breaking associated with increasing speed of the warm beam is clearly evident in Fig. 1 starting from a symmetric picture corresponding to the slow and fast modes having almost identical phase speeds in the forward and backward directions when there is no beam [panel (a)] to highly asymmetric in the presence of a fast beam as seen in panels (f) and (g) in which there are three modes propagating in the forward direction and only one in the backward

direction. This occurs as a result of the directional change of the fast mode from propagation in the backward direction when there is no beam [panel (a)] to the forward direction for higher speeds [panels (b)–(g)].

We proceed now directly to the nonlinear study in which our main interest is on the characteristics of the solitons which occur for high beam speeds.

B. Nonlinear study

We focus our attention in this section on the effect of the warm electron beam on the characteristics of the supported solitons. We treat the electron beam as warm consistent with Berthomier *et al.*¹³ We remind the reader that current neutrality in equilibrium, which requires $N_{bw0}V_{bw0} + N_{bc0}V_{bc0} = 0$, is not satisfied in our single beam model which is similar to the model of Berthomier *et al.*¹³ as there is no cold electron beam ($V_{bc0} = 0$) to oppose the current flow associated with the warm electron beam for which the beam speeds are positive-valued ($V_{bw0} > 0$) as the beam is aligned with the forward direction. A very similar situation arises in the study of ion-acoustic solitons in a model with a single ion beam by Zank and McKenzie.²¹ While large deviations from current neutrality will invalidate the electrostatic approximation, through the generation of currents in Ampère’s law, the magnitudes of the deviations from current neutrality in our study are below unity even for the higher beam speeds, and we consider this effect to be small. In fact, the model with cool, hot, and beam electrons is a very popular one in the literature, as there are several^{31–33} studies using particle-in-cell simulations in which single electron beams are found to excite high frequency electrostatic waves. This highlights the relevance of single electron beams as a source of electrostatic wave emissions in the polar cusp²⁴ region in the magnetosphere and also in the lunar³⁴ environment. Furthermore, there are several reports on studies in the context of laboratory experiments^{35–37} in which ion beam effects on ion-acoustic solitons have been investigated in plasmas, which typically have two ion components, *viz.*, one that is stationary and the other is a beam. The ion beams are not only drivers for the excitation of electrostatic waves in the linear regime but are also responsible for the amplification of solitons in the nonlinear regime. A careful study of the parameters used in Refs. 35–37, reveals that the ion beam densities are quite high and can span up to 80% of the plasma density and the ion beam speed (which is normalized by the ion sound speed) is typically between 1 and 2 but even higher ratios of up to 5 have been used. The normalized beam density $N_{bw} = 0.2$ and beam speed $V_{bw} = 4$ (selecting the largest value in panel (g) in Fig. 1) of the warm (beam) electrons are within the limits of the parameters for the ion beams in the experimental studies, and we consider these acceptable values in our investigation of electrostatic waves.

Returning now to the nonlinear investigation in our own study, the standard plasma parameters are fixed at the same values as in Sec. III A. The linear analysis, which provides insight into solutions of the dispersion relation (8), is a crucial preliminary study in investigating solitons in the nonlinear regime. The dispersion curves ($\omega(k)$) presented in Fig. 1 in this model are based on the dispersion relation (19), which is specific to this model. This was obtained from the general form of the dispersion relation (8) by linearizing the set of Eqs. (2)–(5) in Sec. II A. The $F(M)$ plots are generated using the function defined on the left hand side of Eq. (16). The equivalence of Eqs. (8) and (16) is not surprising as the phase speeds of the linear waves (in the limit of

$K \rightarrow 0$) satisfying $F(M) = 0$ coincide with the minimum speeds required for the existence of solitons in the nonlinear regime which are labeled A–Q in the plots of $F(M)$ in Fig. 2. The explicit forms of the expressions for the Sagdeev pseudopotential $V(\Phi, M)$ and the second

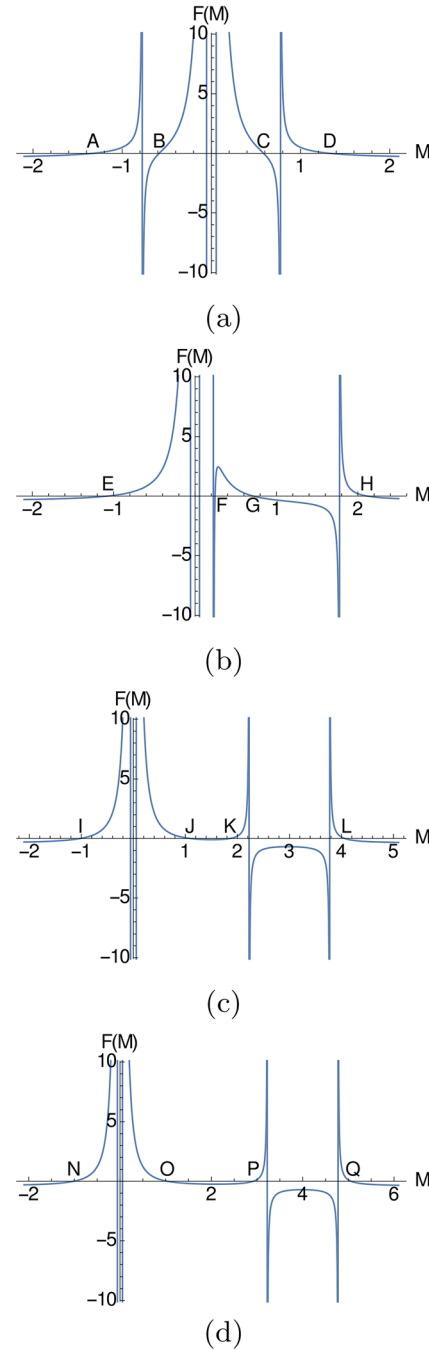


FIG. 2. The dispersion function $F(M)$ for $V_{bw0} = 0$ [panel (a)], 1 [panel (b)], 3 [panel (c)], and 4 [panel (d)]. The fixed parameters are $V_{bc0} = 0.0$, $\sigma_c = 0.001$, $\sigma_{bw} = 0.2$, $N_{h0} = 0.4$, $N_{c0} = 0.4$, and $N_{bw0} = 0.2$.

10 December 2025 10:37:49

derivative $F(M)$ in this model are obtained by replacing “b1” and “b2” in the expressions (14) and (17) with “bw” and “c,” respectively and setting $V_{bc0} = 0$, which is consistent with the dispersion relation in Eq. (19).

We consider first the case in the absence of the beam ($V_{bw0} = 0$). The plot of the dispersion function $F(M)$ in the panel (a) in Fig. 2 is consistent with the dispersion curves in panel (a) in Fig. 1 in which the propagation characteristics of the backward and forward propagating slow and fast waves are found to be approximately symmetrical. There are two backward propagating ($M < 0$) waves, viz., one fast and one slow wave associated with the negative valued critical acoustic speeds labeled A and B, respectively, and there are two forward propagating ($M > 0$) slow and fast waves corresponding to the positive valued critical acoustic speeds labeled C and D, respectively, in panel (a) in Fig. 2.

We shift our attention now to the plots of the Sagdeev pseudopotentials in Fig. 3. The fast electron-acoustic solitons in panel (a) in Fig. 3 propagate for speeds that exceed the value of the higher valued critical acoustic speed $M = 1.3268$ at D in Fig. 2. The amplitude of the supported solitons increases with increasing M above $M = 1.3268$ (solid, black) up to a maximum value of $M = 1.5353$ (dash-dot, blue) beyond which solitons do not occur.

The slow electron-acoustic solitons in panel (b) in Fig. 3, which propagate for lower speeds than the fast solitons, are coincidentally

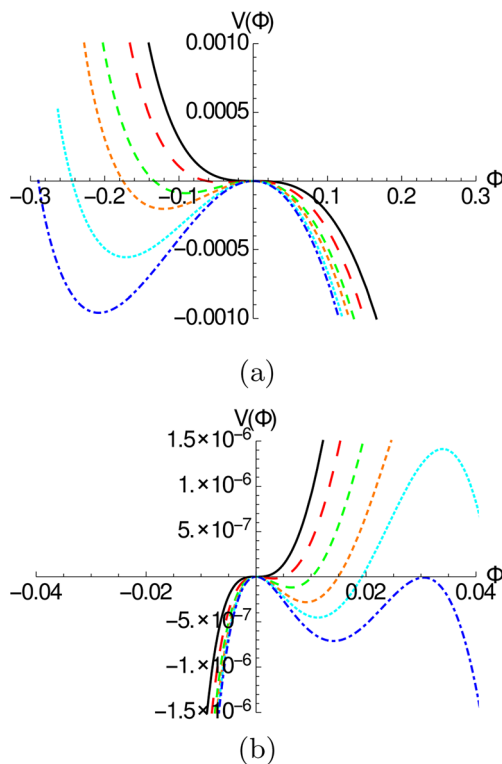


FIG. 3. Sagdeev pseudopotentials for $M = 1.3268$ (solid, black), 1.37 (long dash, red), 1.42 (medium dash, orange), 1.45 (short dash, green), 1.5 (tiny dash, cyan), and 1.5353 (dash-dot, blue) in panel (a). In panel (b) $M = 0.5854$ (solid, black), 0.5870 (long dash, red), 0.5882 (medium dash, orange), 0.589 (short dash, green), 0.5895 (tiny dash, cyan), and 0.59001 (dash-dot, blue). The fixed parameters are $V_{bw0} = 0$, $V_{bc0} = 0$, $\sigma_c = 0.001$, $\sigma_{bw} = 0.2$, $N_{h0} = 0.4$, $N_{c0} = 0.4$, and $N_{bw0} = 0.2$.

found to have positive polarity, which is in agreement with Eq. (18) when there is no beam. This affirms that solitons can switch polarity from negative to positive potential, as has been the main interest of Berthomier *et al.*,¹³ but as it relates to the role of the beam in supporting this. This confirms our claim in the introduction that the inclusion of streaming over and above the retention of inertial effects for the warm electrons is not always necessary for the existence of positive polarity solitons. However, we do not discount the fact that streaming may be necessary for the existence of positive polarity solitons in other parameter regimes such as those discussed by Berthomier *et al.*¹³ The slow solitons propagate for M , which is above $M = 0.5854$ (solid, black) up to a limiting value of $M = 0.59001$ (dash-dot, blue) for which a double layer occurs.

The upper M values where the propagation of the fast and slow solitons terminate are the usual expected limits for the nonlinear structures arising from the breakdown in the density Eq. (11) of the cool or warm electrons when there are no beams ($V_{j0} = 0$, $j = bc, bh$) and the occurrence of a double layer for the slow solitons.

Next we consider a higher beam speed $V_{bw0} = 1.0$ for which $F(M)$ is positive-valued in an intermediate range in M which is between the critical acoustic speeds labeled F and G in panel (b) in our Fig. 2 similar to the dispersion function $H(V)$ in panel (b) in Fig. 1 in Ref. 13. We note the change in sign of the (first) derivative of the function from positive to negative in this portion of $F(M)$ which is of interest to us. On the basis of our results in the linear analysis, we can easily reconcile the behavior of the dispersion function $F(M)$ with the dispersion curves in panel (c) in our Fig. 1, in which we found that the backward propagating fast wave changes direction (orange) and couples with the forward propagating slow wave (blue). This accounts for the double branched nature of the dispersion curves in the regions of small (< 1.569) and large $k\lambda_{de}$ (> 3.895). We remind the reader that in the region of small $k\lambda_{de}$, the fast mode, which changed direction, has not completely overtaken the forward propagating slow mode (orange branch of the dispersion curve for ω_r/ω_{pe} is below the blue branch). However, in the region of large $k\lambda_{de}$ (orange branch of the dispersion curve for ω_r/ω_{pe} is above the blue branch), the fast mode has overtaken the forward propagating slow mode.

We shift attention now to investigate the solitons associated with the linear mode having phase speed labeled F in panel (b) in Fig. 2 which changed direction but has not overtaken the forward propagating slow mode having phase speed labeled G. The solitons are found to have positive polarity in panel (a) in Fig. 4. The nonlinear structures are subsonic and propagate for M values which are below the critical acoustic speed $M = 0.2452$ at F having amplitudes which increase with decreasing M which should vanish at F. However, it is found that the existence of the nonlinear structures is limited by $V(\Phi, M)$ not being defined for negative values of Φ for M values which are smaller than $M = 0.226$. This is a direct violation of the requirement that the pseudopotential must have a local maximum at the origin ($\Phi = 0$) governed by $d^2V(0, M)/d\Phi^2 < 0$, which is necessary for the existence of solitons. We attribute this unusual characteristic of the nonlinear structures to linear instability in the range $1.5689 \leq k\lambda_{de} \leq 3.895$, which is adjacent to the region of small $k\lambda_{de}$ (< 1.569) in panel (c) in Fig. 1. This results in an imbalance between nonlinearity and dispersion, which accounts for the unusual characteristics of the nonlinear structures.

The subsonic character of the wave in the nonlinear regime, as applies to the solitons associated with the phase speed of the linear

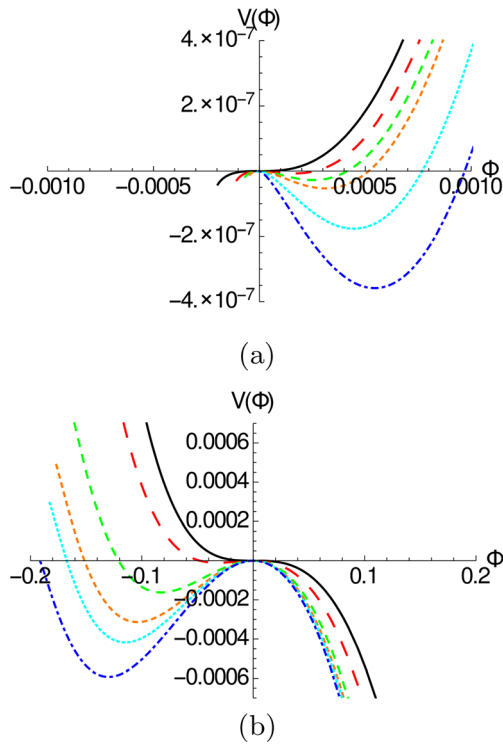


FIG. 4. Sagdeev pseudopotentials for $M = 0.2452$ (solid, black), 0.24 (long dash, red), 0.237 (medium dash, orange), 0.235 (short dash, green), 0.23 (tiny dash, cyan), and 0.226 (dash-dot, blue) in panel (a). In panel (b) $M = 0.7159$ (solid, black), 0.75 (long dash, red), 0.8 (medium dash, orange), 0.82 (short dash, green), 0.83 (tiny dash, cyan), and 0.8435 (dash-dot, blue). The fixed parameters are $V_{bw0} = 1$, $V_{bc0} = 0$, $\sigma_c = 0.001$, $\sigma_{bw} = 0.2$, $N_{h0} = 0.4$, $N_{c0} = 0.4$, and $N_{bw0} = 0.2$.

wave labeled F, is attributed to the change in propagation direction of the linear wave. The solitons associated with the fast mode wave in panel (a) in Fig. 1, which propagates in the backward direction ($\omega_r/\omega_{pe} < 0$ and the wave phase speed $(\omega_r/\omega_{pe})/k\lambda_{de}$ is negative valued) are supersonic when there is no beam, i.e., propagate for speeds that exceed the critical acoustic speed corresponding to the phase speed of the linear wave, i.e., for values of M , which are below the (orange) dispersion curve for ω_r/ω_{pe} . However, when the wave changes propagation direction to the forward direction (now having $\omega_r/\omega_{pe} > 0$ and the wave phase speed $(\omega_r/\omega_{pe})/k\lambda_{de}$ is positive valued) as in panels (f) and (g) in Fig. 1, the M values required for soliton existence which are below the (orange) dispersion curve for ω_r/ω_{pe} are now lower than the critical acoustic speed corresponding to the phase speed of the linear wave, which renders the nonlinear structures subsonic. This is in agreement with our findings that the solitons associated with the wave, which changed direction, and have higher phase speeds labeled K and P for higher V_{bw0} in panels (c) and (d) in Fig. 2, in comparison with F in panel (b), are also subsonic, as will be discussed. It is imperative to point out that the nonlinear structures are still supersonic in the frame of the warm beam electrons guided by the arguments presented by Verheest *et al.*²⁰ on the effects of counterstreaming ion beams on ion-acoustic solitons.

The subsonic nature of nonlinear structures has already been alluded to in Refs. 19–21 as applies to ion-acoustic waves for a dispersion function which is negative-valued for the range of M -values between the critical acoustic speeds in which the derivative of the function changes sign from negative to positive similar to the behavior of $F(M)$ which occurs for higher beam speeds as seen in panel (c) in Fig. 2. An interesting finding in this study is that the occurrence of a dispersion function which is positive-valued for the range of M -values between the pair of critical acoustic speeds in which the derivative of the function changes sign from positive to negative [panel (b) in Fig. 2] can be reconciled with dispersion curves which are double-branched in the regions of both small and large $k\lambda_{de}$ as observed in panel (c) in Fig. 1. This situation appears to arise only in plasma models which are asymmetric as in the single beam model investigated by Berthomier *et al.*¹³ (Sec. III in this paper) and the model with asymmetric counterstreaming electron beams (Sec. IV in this paper) but not in plasma models with symmetric electron beams (Sec. V in this paper and in the study with symmetric counterstreaming ion beam components in Ref. 19). Our initial interest in the study was to investigate the generation of subsonic solitons associated with a dispersion function which is negative-valued for the range of M -values between the pair of critical acoustic speeds [labeled J and K in panel (c) in Fig. 2 or O and P in panel (d)] in which the derivative of the function changes sign from negative to positive, for which the modes which were coupled for lower beam speeds have uncoupled and the dispersion curves which were double-branched have separated and are distinct for higher beam speeds [cf. dispersion curves in panels (f) and (g) in Fig. 1]. However our detailed investigation of the effects of the beams on the dispersion curves, which is included here, provides broad insights relating to the characteristics of the linear waves which was not investigated in the paper by Berthomier *et al.*¹³ such as how the dispersion curves differ when the dispersion function is positive-valued as opposed to negative-valued for the range of M -values between the critical acoustic speeds in which the derivative of the function changes sign.

Returning to our results, we refer the reader now to plots of Sagdeev potentials in panel (b) in Fig. 4 corresponding to the solitons associated with the linear mode with phase speed labeled G in panel (b) in Fig. 2. These solitons which are supersonic, propagate for speeds which are above $M = 0.7159$ (solid black) in panel (b) in Fig. 4 up to a well defined upper limit for solitons $M = 0.8435$ (dash-dot, blue) associated with breakdown in the density of the warm beam electrons (11) or the cool non-drifting ($V_{bc0} = 0$) electrons.

We note the evolution in the dispersion function $F(M)$ from positive-valued for the range of M -values between the critical acoustic speeds (labeled F and G) in which the derivative of the function changes sign from positive to negative for $V_{bw0} = 1$ [panel (b) in Fig. 2] to negative-valued for the range of M -values between the critical acoustic speeds (labeled J and K) in which the derivative of the function changes sign from negative to positive for a higher $V_{bw0} = 3$ [panel (c) in Fig. 2]. The linear mode which has changed direction has overtaken the slow mode which is labeled J in panel (c) in Fig. 2 and has the higher phase speed labeled K for a higher $V_{bw0} = 3$ in panel (c) in Fig. 2. The two modes have uncoupled noting that the dispersion curves denoted in blue and orange have separated and are now distinct in panel (f) in Fig. 1. The nonlinear structures in this high beam speed regime for which $F(M)$ is negative-valued for the range of M -values between the pair of critical acoustic speeds in which the derivative of

the function changes sign from negative to positive, corresponds to a situation in which the linear modes are stable. This follows the intermediate beam speed regime in which the two linear modes which are coupled are unstable (and damped). Our results based on a study in a different plasma context with inertial electron components of which one is a drifting electron beam component, are in complete agreement with the results of Zank and McKenzie²¹ for low frequency phenomena, in which paper it is explicitly stated that the condition for the existence of three forward propagating ion-acoustic solitons associated with three forward propagating waves is the absence of linear instabilities.

The solitons associated with J are supersonic and propagate for M increasing above $M = 1.0959$ (solid, black) at J, to $M = 1.2$ (long dash, red), $M = 1.3$ (medium dash, orange) and $M = 1.5$ (short dash, green) as observed in Fig. 5. These have amplitudes which increase with increasing M . This is immediately followed by the propagation of the second group of solitons associated with the higher valued critical acoustic speed K which are subsonic and therefore propagate for M values below K because of the directional change of the linear wave. These have amplitudes that diminish for increasing M , as observed for $M = 1.7$ (tiny dash, cyan), which has lower amplitude than the soliton that occurs for $M = 1.5$ (short dash, green), which terminates at $M = 1.8580$ (dash-dot, blue) at K in Fig. 5. This confirms that soliton propagation is continuous in the range in M between the critical acoustic speeds at J and K.

We finally consider the effect of $V_{bw0} = 4$ in Fig. 6, which is higher than $V_{bw0} = 3$ in Fig. 5. We note there is not much change in the dispersion curves when V_{bw0} increases from $V_{bw0} = 3$ in panel (f) to $V_{bw0} = 4$ in panel (g) in Fig. 1, except that the phase speeds are higher for $V_{bw0} = 4$. The phase speeds of the linear modes labeled O and P in panel (d) in Fig. 2 correspond, respectively, to the forward propagating slow mode and the fast mode that changed direction. Consequently, the solitons associated with O and P are supersonic and subsonic, respectively. The solitons associated with O, therefore, propagate for M that exceed the value $M = 1.0334$ (solid, black) at O and terminates at $M = 1.7590$ (dash-dot, blue) in panel (a) in Fig. 6. The propagation of the second group of solitons associated with P, which are subsonic, and therefore, propagate for M values that are below P starts just above $M = 2.797$ (dash-dot, blue) having amplitudes, which diminish for increasing M , and terminates at $M = 2.9200$ (solid, black) at P, as observed in panel (b) in Fig. 6. This results in the

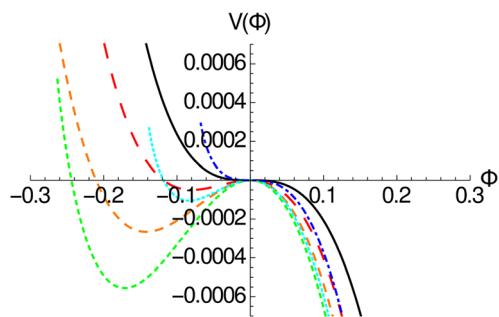


FIG. 5. Sagdeev pseudopotentials for $M = 1.0959$ (solid, black), 1.2 (long dash, red), 1.3 (medium dash, orange), 1.5 (short dash, green), 1.7 (tiny dash, cyan), and 1.8580 (dash-dot, blue). The fixed parameters are $V_{bw0} = 3$, $V_{bc0} = 0$, $\sigma_c = 0.001$, $\sigma_{bw} = 0.2$, $N_{h0} = 0.4$, $N_{c0} = 0.4$, and $N_{bw0} = 0.2$.

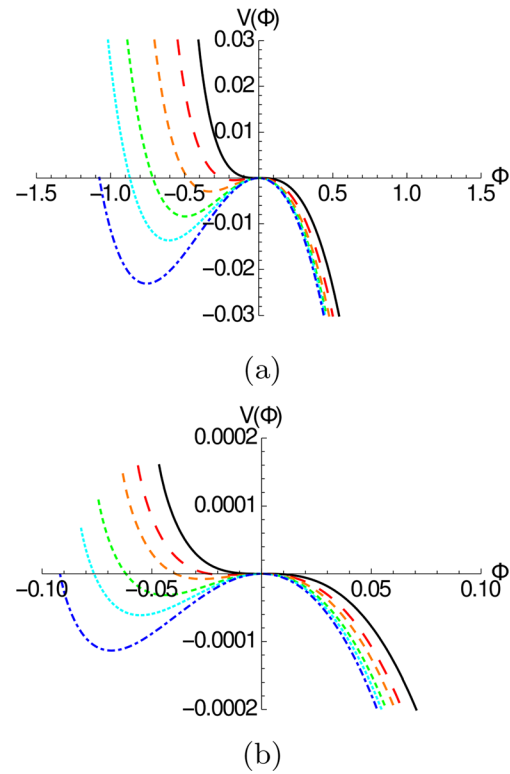


FIG. 6. Sagdeev pseudopotentials for $M = 1.0334$ (solid, black), 1.2 (long dash, red), 1.35 (medium dash, orange), 1.5 (short dash, green), 1.6 (tiny dash, cyan), and 1.7590 (dash-dot, blue) are shown in panel (a). In panel (b) Sagdeev pseudopotentials are shown for $M = 2.9200$ (solid, black), 2.89 (long dash, red), 2.87 (medium dash, orange), 2.84 (short dash, green), 2.82 (tiny dash, cyan), and 2.797 (dash-dot, blue). The fixed parameters are $V_{bw0} = 4$, $V_{bc0} = 0$, $\sigma_c = 0.001$, $\sigma_{bw} = 0.2$, $N_{h0} = 0.4$, $N_{c0} = 0.4$, and $N_{bw0} = 0.2$.

occurrence of a stopband range of M values for which no solitons propagate, which starts at $M = 1.7590$ and terminates at $M = 2.797$ and lies between the two critical acoustic speeds O and P. This differs in contrast to the effect of a lower beam speed $V_{bw0} = 3$ for which soliton propagation is continuous in M between the two critical acoustic speeds at J and K in panel (c) in Fig. 2.

IV. MODEL WITH COUNTER-STREAMING ELECTRON BEAMS (ASYMMETRIC)

A. Linear analysis

We now shift to a plasma model with counterstreaming electron beams, which are asymmetric as the beams have different temperatures and densities. The warm ($j = bw$) and cool ($j = bc$) beams are aligned with the forward and backward directions, respectively. The dispersion relation specific to this model given by

$$\frac{N_{bc0}}{(\Omega - KV_{bc0})^2 - 3K^2\sigma_{bc}} + \frac{N_{bw0}}{(\Omega - KV_{bw0})^2 - 3K^2\sigma_{bw}} - \frac{N_{h0}}{K^2} - 1 = 0, \quad (20)$$

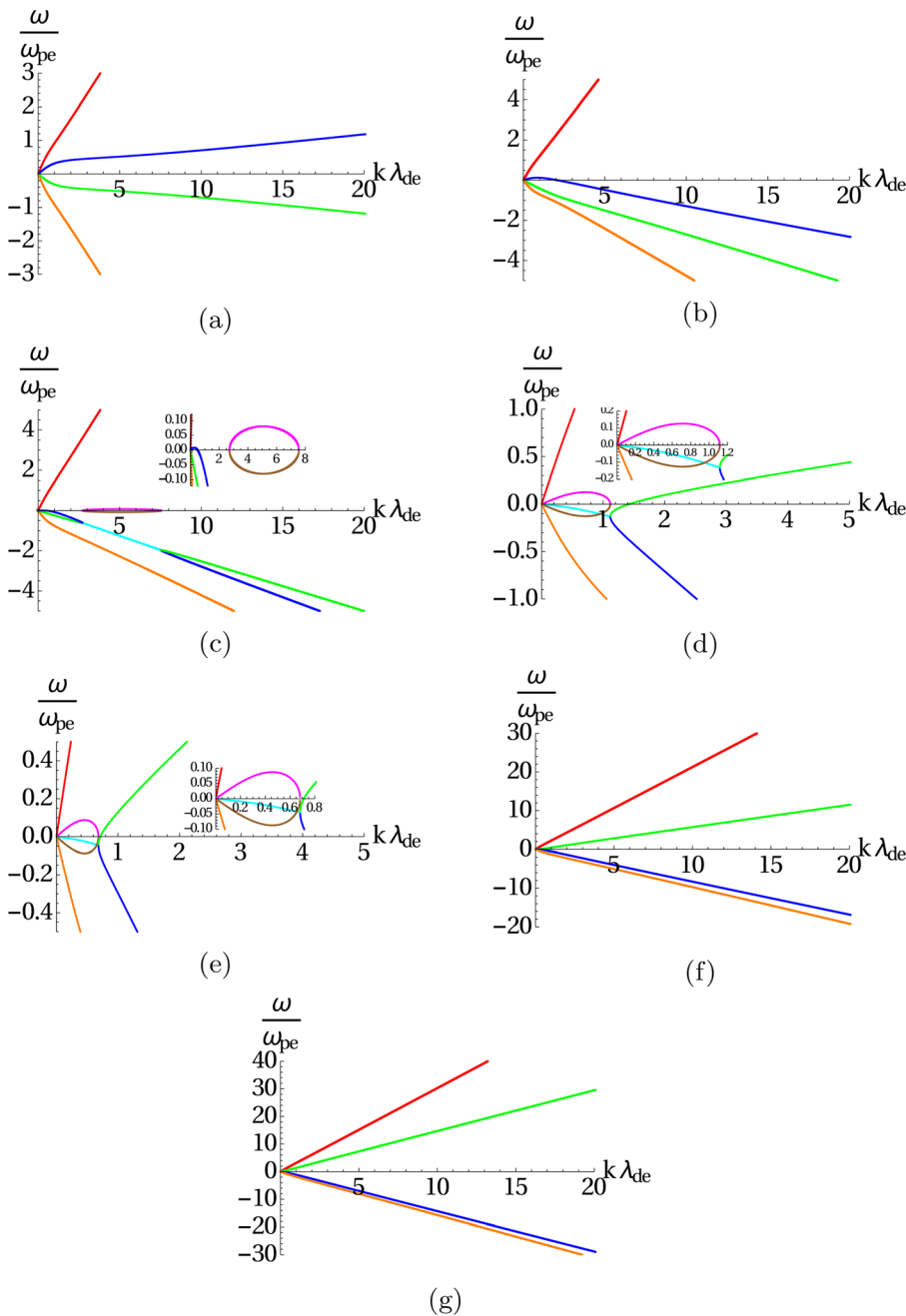


FIG. 7. Dispersion curves for the real frequency ω_r/ω_{pe} (red, blue, orange, green, cyan) and growth (magenta) and damping rate (brown) γ/ω_{pe} for (a) $V_{bw0} = 0$ and $V_{bc0} = 0$, (b) $V_{bw0} = 0.3$ and $V_{bc0} = -0.2$, (c) $V_{bw0} = 0.525$ and $V_{bc0} = -0.35$, (d) $V_{bw0} = 0.87$ and $V_{bc0} = -0.58$, (e) $V_{bw0} = 1.05$ and $V_{bc0} = -0.7$, (f) $V_{bw0} = 1.35$ and $V_{bc0} = -0.9$, and (g) $V_{bw0} = 2.25$ and $V_{bc0} = -1.5$. The insets provide magnified views of the regions of instability and damping. The fixed parameters are $\sigma_{bc} = 0.001$, $\sigma_{bw} = 0.2$, $N_{h0} = 0.5$, $N_{bc0} = 0.2$, and $N_{bw0} = 0.3$.

10 December 2025 10:37:49

was obtained from the general dispersion relation for a plasma with counterstreaming beams [Eq. (9)], by replacing the subscripts “b1” and “b2” with “bw” and “bc,” respectively.

The parameters are fixed at the values $\sigma_{bc} = 0.001$ and $\sigma_{bw} = 0.2$ and $N_{bc0} = 0.2$ and $N_{bw0} = 0.3$, respectively, for the temperatures and densities of the cool and warm beam electrons. The cool and warm electron beams are assumed to be aligned with the backward and forward

directions, respectively, having speeds which are denoted by $V_{bc0} (< 0)$ and $V_{bw0} (> 0)$.

In investigating the effects of counterstreaming electron beams, we will assume that current neutrality, *viz.*, $N_{bw0}V_{bw0} + N_{bc0}V_{bc0} = 0$ is satisfied in equilibrium as this offers some variation from the previous model that will allow us to assess whether the assumption of a current neutral condition in equilibrium will invoke significant differences

in wave characteristics in contrast to nonzero-current conditions in equilibrium synonymous with the plasma model with the single electron beam in Sec. III, in which there is a net current associated with the finite drift speed of the warm beam electrons. Having fixed the densities and temperatures of the cool and warm electron beams at $N_{bc0} = 0.2$ and $N_{bw0} = 0.3$, respectively, we have carefully selected the combination of the cool and warm electron beam speeds to satisfy $N_{bw0}V_{bw0} + N_{bc0}V_{bc0} = 0$ so that current neutrality prevails in equilibrium.

We again start with the situation with no beams in panel (a) in Fig. 7. There are two slow and two fast modes. The slow (and fast) mode denoted in blue (and red) having $\omega_r/\omega_{pe} > 0$ propagates in the forward direction. The slow (and fast) mode denoted in green (and orange) having $\omega_r/\omega_{pe} < 0$ propagates in the backward direction.

We observe in Fig. 7 that for increasing speed of both the warm and cool electron beams denoted V_{bw0} and V_{bc0} , respectively, the phase speed of both the forward (blue) and backward propagating (green) slow mode waves [panel (a)] which are most sensitive to increasing speed of the backward and forward aligned cool and warm electron beam, respectively, decrease and eventually change directions to propagation in the backward and forward directions, respectively, [panels (d)–(g)].

The two slow modes, which are most sensitive to the speed of the counterstreaming beams, have now coupled in panel (c) as evident from the dispersion curve, which is double-branched in ω_r/ω_{pe} in regions of small (< 2.71) and large $k\lambda_{de}$ (> 7.549). These regions lie on either side of an intermediate region in $k\lambda_{de}$ ($2.71 \leq k\lambda_{de} \leq 7.549$) where wave growth (and damping) of the slow modes occur which coincides with the single-branched portion of the dispersion curve in ω_r/ω_{pe} (cyan). We point out here that the slow mode (blue) has not yet passed the slow mode (green) in the region of small $k\lambda_{de}$ (< 2.71) as the blue portion of the dispersion curve in ω_r/ω_{pe} is still above the green branch of the dispersion curve. However the slow mode corresponding to the blue curve has passed the slow mode corresponding to the green curve in the region of large $k\lambda_{de}$ (> 7.549) where the blue branch of the dispersion curve in ω_r/ω_{pe} is below the green branch.

We observe that the two modes, which are coupled in panel (c) in Fig. 7, start to decouple for higher speeds for the warm and cool electron beams. The $k\lambda_{de}$ range over which instability (and damping) occurs diminishes for the combination of higher values of $V_{bw0} = 0.87$ and $V_{bc0} = -0.58$ [panel (d)] and this range diminishes further for $V_{bw0} = 1.05$ and $V_{bc0} = -0.7$ [panel (e)]. The decoupling is complete for higher combinations of $V_{bw0} = 1.35$ and $V_{bc0} = -0.9$ in panel (f) and $V_{bw0} = 2.25$ and $V_{bc0} = -1.5$ in panel (g). The slow modes that were propagating in the forward (blue) and backward directions (green) when there are no beams ($V_{bc0} = V_{bw0} = 0$, panel (a)) have now changed propagation directions to the backward and forward directions, respectively.

Looking ahead to the plots of the dispersion function $F(M)$ for $V_{bw0} = 0.525$ and $V_{bc0} = -0.35$ in panel (a) in Fig. 8, we point out that the solitons associated with the linear mode with phase speed labeled F can then be reconciled with the branch of the dispersion curve which is shown in green in the region of small $k\lambda_{de}$ in panel (c) in Fig. 7. The linear mode with phase speed that is labeled G can be reconciled with the branch of the dispersion curve which is shown in blue in the region of small $k\lambda_{de}$.

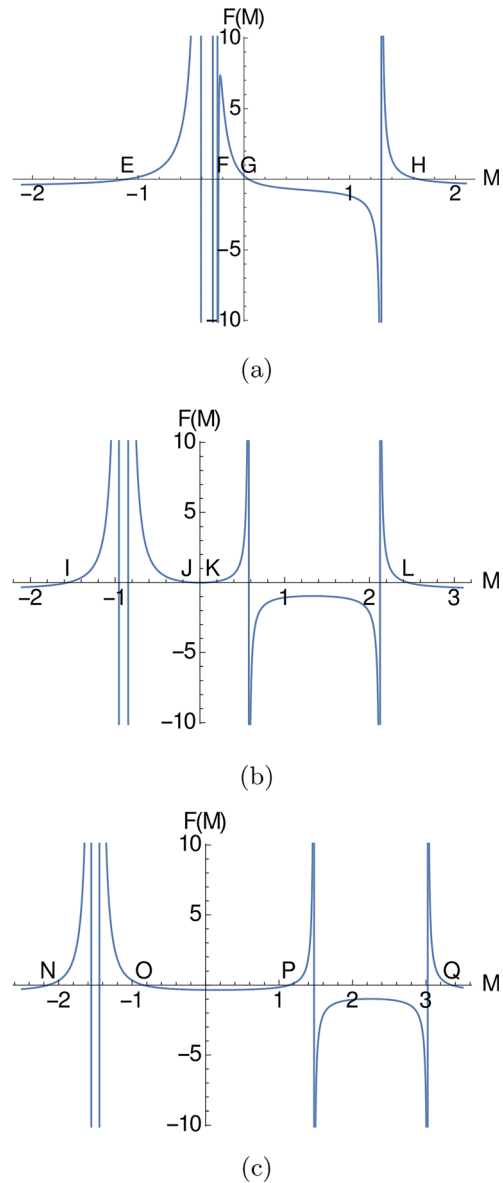


FIG. 8. The dispersion function $F(M)$ for $V_{bw0} = 0.525$ and $V_{bc0} = -0.35$ [panel (a)], $V_{bw0} = 1.35$ and $V_{bc0} = -0.9$ [panel (b)] and $V_{bw0} = 2.25$ and $V_{bc0} = -1.5$ [panel (c)]. The fixed parameters are $\sigma_{bc} = 0.001$, $\sigma_{bw} = 0.2$, $N_{h0} = 0.5$, $N_{bc0} = 0.2$, and $N_{bw0} = 0.3$.

These two waves pass each other uncoupling and the critical acoustic speed F (or G) can then be reconciled with the higher phase speed modes labeled K (or J) for $V_{bw0} = 1.35$ and $V_{bc0} = -0.9$ in panel (b) in Fig. 8 and P (or O) for $V_{bw0} = 2.25$ and $V_{bc0} = -1.5$ in panel (c) in Fig. 8 corresponding to the green (or blue) dispersion curve in panels (f) and (g) in Fig. 7. Both waves have reversed propagation directions for high beam speeds in panels (f) and (g) in Fig. 7 in comparison with panel (a) when there are no beams.

We conclude this section by pointing out that an increase in the speed of the two counterstreaming beams on the waves is qualitatively very similar to the effect of increasing the speed of the warm electron beam on the waves in the case of the single beam model. There are subtle differences as it is the fast mode which changes propagation direction from the backward to forward direction and couples with the forward propagating slow wave in the single beam model. Here in the model with asymmetric counterstreaming beams, it is the slow mode that has changed propagation direction from the forward to the backward direction and couples with the backward propagating slow mode. Nevertheless, the observed coupling to decoupling of the waves is very similar in both models. The similarities are found to extend to the nonlinear regime.

B. Nonlinear study

Moving to the nonlinear study in a plasma configuration with counterstreaming beams, which are asymmetric, the effect of the two beams appears to be consistent with the single beam results discussed earlier. The relevant expressions for $V(\Phi, M)$ and $F(M)$ in this model are obtained by replacing subscripts “b1” and “b2” in Eqs. (14) and (17) with “bw” and “bc,” respectively.

We will consider first the combination $V_{bw0} = 0.525$ and $V_{bc0} = -0.35$ for the speeds of the counterstreaming beams for which the dispersion function $F(M)$ is positive-valued for the range of M -values between the critical acoustic speeds as observed in panel (a) in Fig. 8. The critical acoustic speeds labeled F and G occur at $M = -0.2407$ and $M = 0.0440$, respectively. We reconcile this situation with the dispersion curve for ω_r/ω_{pe} in panel (c) in Fig. 7, in which, the slow mode, which propagates in the forward direction (blue) when there are no beams, has changed direction for large $k\lambda_{de}$ (> 0.5) and couples with the backward propagating slow mode wave (green). There is still a region of small $k\lambda_{de}$ (< 0.5) where the wave propagates in the forward direction. The two slow modes have not yet passed each other and the green branch of the dispersion curve is still below the blue branch in the region of small $k\lambda_{de}$ (< 2.71), but is above the blue branch in the region of large $k\lambda_{de}$ (> 7.549). The solitons associated with F can be reconciled with the linear mode, which corresponds to the green branched portion of the dispersion curve for which the phase speed is negative valued. The solitons associated with G, on the other hand, can be reconciled with the linear mode that corresponds to the blue branch portion of the dispersion curve, which has a phase speed that is positive (negative)-valued for $k\lambda_{de} < 0.5$ (> 0.5).

The Sagdeev pseudopotentials associated with F and G are not shown, as the properties of the nonlinear structures are quite similar to those in the earlier model, except that the nonlinear structures associated with F are supersonic in this model. It is found that these structures do not occur for large values of M as $V(\Phi, M)$ becomes undefined on the side of negative values of Φ such that $V(\Phi, M)$ does not have a local maximum at $\Phi = 0$. This is because the nonlinear structures are associated with the branch of the dispersion curve, which is unstable for intermediate $k\lambda_{de}$ ($2.71 \leq k\lambda_{de} \leq 7.549$) that is directly adjacent to the region of small $k\lambda_{de}$ where the phase speed of the wave occurs. The nonlinear structures associated with G, on the other hand, do not exhibit the characteristic that $V(\Phi, M)$ becomes undefined on the side of negative values of Φ , as these are associated with the (stable) branch of the dispersion curve that is damped in the range of intermediate $k\lambda_{de}$.

The two slow modes have decoupled for higher speeds $V_{bw0} = 1.35$ and $V_{bc0} = -0.9$ for the counterstreaming electron beams, and the propagation directions of the slow mode waves are reversed in comparison to when there are no beams or for very low beam speeds. The solitons associated with the phase speeds of the linear modes labeled J and K in panel (b) in Fig. 8 can be reconciled with the two slow modes that have changed direction in panel (f) in Fig. 7. The slow mode (green) has now uncoupled from the slow mode shown in blue and the slow modes shown in blue (and green) have changed propagation directions to the backward (and forward) directions. The waves have higher phase speeds labeled O and P for higher beam speeds in panel (c) in Fig. 8, which can be reconciled with the dispersion curves in panel (g) in Fig. 7.

It is the directional change of both the backward and forward propagating slow modes that renders the nonlinear soliton structures subsonic for sufficiently high beam speeds as the phase speeds required for soliton existence, which are below (or above) the green (or blue) dispersion curve when there are no beams [Fig. 7(a)] are lower than the critical acoustic speeds when the wave changes direction to the forward (or backward) direction [panels (f) and (g) in Fig. 7].

Consequently, the two groups of solitons associated with critical acoustic speeds J and K for $V_{bw0} = 1.35$ and $V_{bc0} = -0.9$ [panel (b) in Fig. 8] and O and P for the higher $V_{bw0} = 2.25$ and $V_{bc0} = -1.5$ [panel (c) in Fig. 8] are subsonic. The results are very similar to those of the earlier model in that soliton propagation is found to be continuous in the range in M between the critical acoustic speeds for lower beam speeds (above a critical value); however, a stopband range of non-admissible soliton speeds occurs for higher beam speeds. The main difference in comparison with the results of the earlier model with a single electron beam is that the two groups of solitons associated with the pair of critical acoustic speeds propagate in opposite directions in the model with asymmetric counterstreaming beams. The solitons associated with J propagate in the backward direction for values of M which are below $M = -0.0567$ at J, and have amplitudes which increase for decreasing magnitude of M to just below $M = 0$ as revealed by the Sagdeev pseudopotentials in Fig. 9. This is followed by the propagation of the second group of solitons in the forward direction having amplitudes that diminish for M increasing above $M = 0$ to vanishing of the solitons at $M = 0.0615$ at K. In the ion rest frame, soliton propagation also occurs for $M = 0$ where the amplitude of the

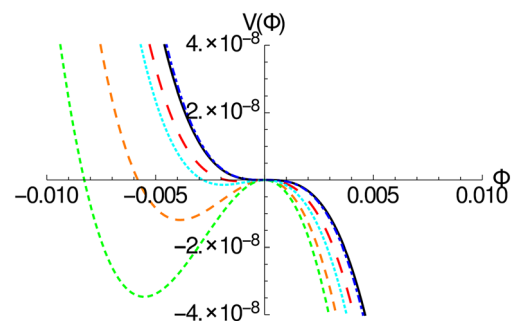


FIG. 9. Sagdeev pseudopotentials for $M = -0.0567$ (solid, black), -0.05 (long dash, red), -0.03 (medium dash, orange), 0.0 (short dash, green), 0.05 (tiny dash, cyan), and 0.0615 (dash-dot, blue). The fixed parameters are $V_{bw0} = 1.35$, $V_{bc0} = -0.9$, $\sigma_{bc} = 0.001$, $\sigma_{bw} = 0.2$, $N_{i0} = 0.5$, $N_{bc0} = 0.2$, and $N_{bw0} = 0.3$.

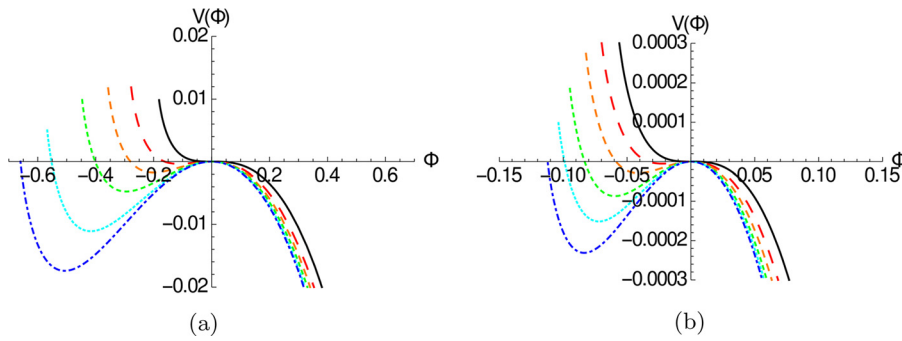


FIG. 10. Sagdeev pseudopotentials for $M = -0.8430$ (solid, black), -0.7 (long dash, red), -0.6 (medium dash, orange), -0.5 (short dash, green), -0.38 (tiny dash, cyan), and -0.2966 (dash-dot, blue). In panel (b) $M = 1.1380$ (solid, black), 1.1 (long dash, red), 1.07 (medium dash, orange), 1.04 (short dash, green), 1.02 (tiny dash, cyan), and 1.002 (dash-dot, blue). The fixed parameters are $V_{bw0} = 2.25$, $V_{bc0} = -1.5$, $\sigma_{bc} = 0.001$, $\sigma_{bw} = 0.2$, $N_{h0} = 0.5$, $N_{bc0} = 0.2$, and $N_{bw0} = 0.3$.

nonlinear structures is maximum, and at which value the separation of the M regimes for the backward and forward propagating solitons occurs. This reveals that soliton propagation is continuous in the range in M between the critical acoustic speeds at J and K in Fig. 8.

This differs in contrast to the propagation characteristics of the solitons associated with O and P for the higher $V_{bw0} = 2.25$ and $V_{bc0} = -1.5$. The backward propagating solitons which propagate below $M = -0.8430$ at O which have amplitudes which increase for diminishing M terminates at $M = -0.2966$ as seen in panel (a) in Fig. 10. The forward propagating solitons for which the propagation starts just above $M = 1.002$ which have amplitudes which diminish for increasing M terminates at $M = 1.1380$ at P as observed in panel (b) in Fig. 10. This yields a stopband range in non-admissible soliton speeds which starts at $M = -0.2966$ and terminates at $M = 1.002$ between the critical acoustic speeds O and P, which is consistent with the findings in the high beam speed regime in the earlier model.

V. MODEL WITH COUNTER-STREAMING ELECTRON BEAMS (SYMMETRIC)

A. Linear analysis

We consider here a plasma configuration with counterstreaming electron beams that are symmetric (have the same density, temperature, and speed). The dispersion relation specific to this model corresponds exactly to the expression (9). The beam, which is aligned with the forward or backward direction, respectively, has a speed that is denoted by $V_{b10} (>0)$ or $V_{b20} (<0)$. The densities and temperatures of the beams are fixed at the values $N_{b10} = 0.3$, $N_{b20} = 0.3$ and $\sigma_{b1} = 0.2$ and $\sigma_{b2} = 0.2$, respectively, for the forward and backward aligned electron beams and the hot electron density is fixed at $N_{h0} = 0.4$.

We again start with the situation with no beams corresponding to the combination $V_{b10} = 0$ and $V_{b20} = 0$ in panel (a) in Fig. 11. We observe that the slow modes are absent when the thermal speeds of the two beam components are identical. The two fast modes that propagate in the forward and backward directions correspond to the dispersion curves for ω_r/ω_{pe} shown in red and orange, respectively.

For finite values of the speed of the forward and backward aligned beams corresponding to $V_{b10} = 0.5$ and $V_{b20} = -0.5$, respectively, in panel (b) we note the appearance of the two slow mode waves with real frequencies denoted by the blue and green curves, which propagate in the forward and backward direction, respectively.

For a higher combination of speeds $V_{b10} = 0.8$ and $V_{b20} = -0.8$ in panel (c), we note that $\omega_r/\omega_{pe} = 0$ for the two slow mode waves, one of which has a positive valued imaginary part γ/ω_{pe} and the other a negative valued imaginary part in the region of small $k\lambda_{de}$ (< 3.82).

These are “zero frequency” modes of which one is purely growing ($\gamma/\omega_{pe} > 0$) and the other damped ($\gamma/\omega_{pe} < 0$) denoted by the curves shown in magenta and brown, respectively. However, ω_r/ω_{pe} is finite valued outside the region where instability (and damping) occurs.

The range of $k\lambda_{de}$ values over $\omega_r/\omega_{pe} = 0$ for the two slow modes, which coincides with where instability (and damping) occurs, now diminishes over the range $k\lambda_{de} < 1.592$ for a higher $V_{b10} = 0.9$ and $V_{b20} = -0.9$ [panel (d)]. The phase speeds of the two slow modes outside the region, where instability (and damping) occurs, are higher for $V_{b10} = 0.9$ and $V_{b20} = -0.9$ in panel (d) than in panel (c).

For a higher $V_{b10} = 1.5$ and $V_{b20} = -1.5$ [panel (e)] the regime for instability (and damping) vanishes and finite valued solutions for ω_r/ω_{pe} are obtained over the entire range in $k\lambda_{de}$ for the forward and backward propagating slow mode waves. The behavior is very similar for an even higher $V_{b10} = 3$ and $V_{b20} = -3$ in panel (f) except that the wave phase speeds are higher than in panel (e). A very similar symmetrical picture for the propagation characteristics of the backward and forward propagating slow and fast ion-acoustic waves was reported to arise in the model with symmetric counterstreaming ion beams by Lakhina *et al.*¹⁹

It is very tempting to conclude that there is no directional change of the two slow modes in the symmetric model because of perfect symmetry in the propagation characteristics of the backward and forward propagating slow (and fast) modes. The directional change of the two modes would be difficult to detect unless the two modes have asymmetric propagation characteristics. However, with the insights gained from the earlier models with a single and asymmetric counterstreaming electron beams, which, respectively, were found to support the directional change of one and two wave modes, we have swapped the colors of the forward and backward propagating slow modes (green with blue and blue with green) in panels (d), (e), and (f) in Fig. 11 to indicate the directional change of the backward and forward propagating slow modes which has occurred for the higher combinations of beam speeds in comparison with lower beam speeds in panels (b) and (c). The understanding that the two slow mode waves have changed direction is also evident in the nonlinear regime through the observed subsonic character of solitons associated with the two modes for higher beam speed combinations, which is discussed in Sec. V B.

B. Nonlinear study

Shifting attention to the nonlinear study in the model with symmetric counterstreaming beams, the expressions for the Sagdeev

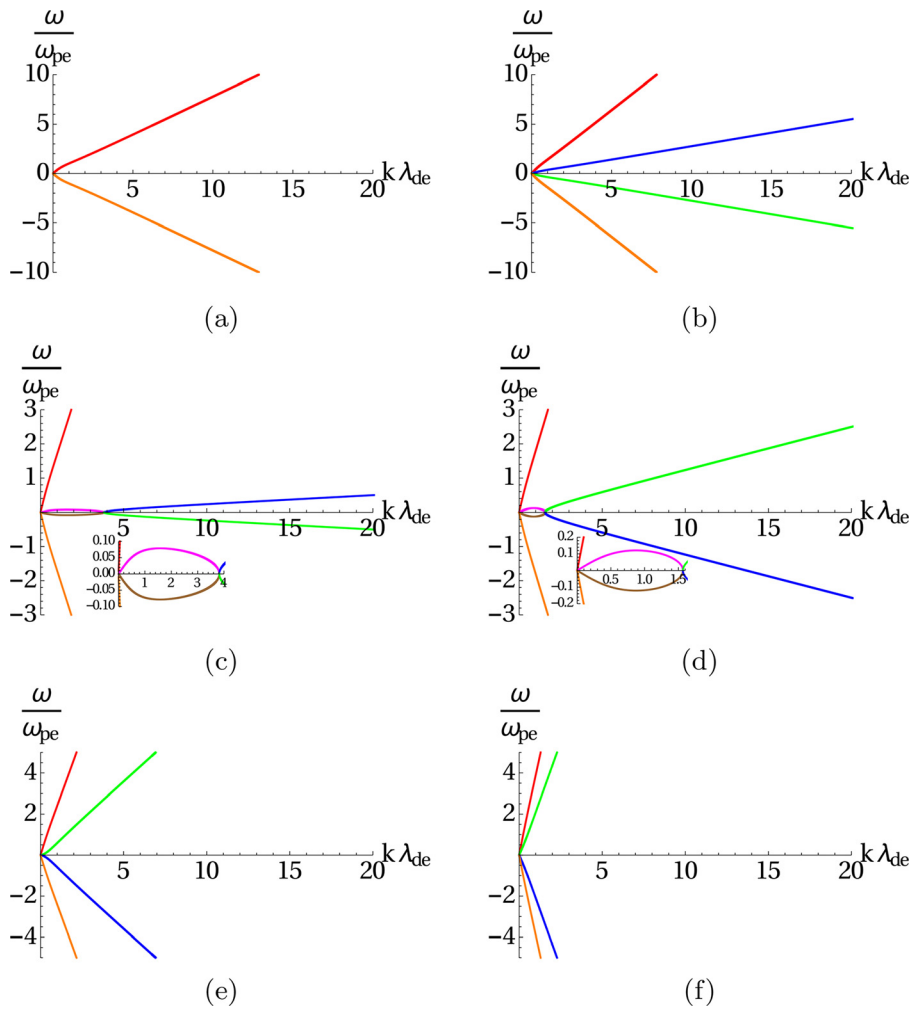


FIG. 11. Dispersion curves for the real frequency ω_r/ω_{pe} (red, blue, orange, green) and growth (magenta) and damping rate (brown) γ/ω_{pe} for (a) $V_{b10} = 0$ and $V_{b20} = 0$, (b) $V_{b10} = 0.5$ and $V_{b20} = -0.5$, (c) $V_{b10} = 0.8$ and $V_{b20} = -0.8$, (d) $V_{b10} = 0.9$ and $V_{b20} = -0.9$, (e) $V_{b10} = 1.5$ and $V_{b20} = -1.5$, and (f) $V_{b10} = 3$ and $V_{b20} = -3$. The insets provide magnified views of the regions of instability and damping. The fixed parameters are $\sigma_{b1} = 0.2$, $\sigma_{b2} = 0.2$, $N_{b0} = 0.4$, $N_{b10} = 0.3$, and $N_{b20} = 0.3$.

pseudopotential $V(\Phi, M)$ and $F(M)$, respectively, correspond exactly to the expression (14) and the left hand side of (17). The consideration of counterstreaming electron beams which are symmetric (have the same density, temperature and speed) invokes symmetry in the plasma system such that the critical acoustic speeds of the backward and forward propagating slow mode waves now have the same magnitude in contrast to the case of asymmetric beams in Sec. IV. We have not included the relevant figures of the dispersion function $F(M)$ and associated Sagdeev pseudopotentials for this model as the figures are very similar to those shown for the earlier model with asymmetric counterstreaming beams.

The dispersion function $F(M)$ is never positive-valued but only negative-valued for a range of M -values in which the derivative of the function changes sign, in the model with symmetric counterstreaming beams. The nonlinear structures in this model have similar characteristics as the nonlinear structures which were found to be supported in the previous model with asymmetric counterstreaming electron beams in that while there is no stopband between the M regimes for the backward and forward propagating solitons for low combinations of equal speeds for the counterstreaming electron beams, a stopband arises

between the critical acoustic speeds for high combinations of equal beam speeds. The subsonic nature of both groups of solitons associated with the pair of critical acoustic speeds in the low and high beam speed regimes corroborates the directional changes of the two slow mode waves which we had alluded to in the linear analysis in Sec. V A. The directional changes would be difficult to detect due to the symmetric propagation characteristics of the two slow mode waves in the model with symmetric counterstreaming beams. We remind the reader that we swapped the colors of the dispersion curves for ω_r/ω_{pe} for the backward and forward propagating slow mode waves in panels (d), (e), and (f) in comparison with panels (b) and (c) in Fig. 11.

These results are consistent with the results of the earlier models with asymmetric counterstreaming beams in Sec. IV and the single warm electron beam in Sec. III. In comparing the results in the different models, the main difference is that for sufficiently high beam speeds for which $F(M)$ is negative-valued for a range of M -values in which the derivative of the function changes sign, only one group of solitons which are associated with the pair of critical acoustic speeds is subsonic in the model with a single beam which is attributed to the directional change of only one of the wave modes. This differs in

contrast to the models with asymmetric or symmetric counterstreaming beams in which both groups of solitons are subsonic which are associated with the directional changes of the two slow mode waves.

VI. CONCLUSIONS

Our main objective in this paper was to investigate the effect of high speed electron beams in the generation of nonlinear soliton structures which are subsonic in models with two species of adiabatic electrons, Boltzmann hot electrons, and a single ion species, the dynamics of which are not considered. One or both of the inertial electron species are modeled as drifting (beam) components. We started with the model with a single warm electron beam consistent with that of Berthomeier *et al.*¹³ and extended the studies to models with counterstreaming electron beams which are asymmetric and symmetric.

As a prequel to the nonlinear studies for the three models the linear analyses have been conducted to investigate the explicit effect of beam speed on the dispersion curves ω_r/ω_{pe} ($\equiv \Omega$) plotted as a function of the normalized wave number $k\lambda_{de}$ ($\equiv K$). The effect of increasing speed of the single electron beam or both asymmetric beam components in the model with counterstreaming electron beams was found to have the effect of supporting the directional change(s) of one (or two) wave modes, which couple with the slow mode propagating in the opposite direction. For intermediate beam speeds it is found that there are regions in K where there is instability (and damping) for the two wave modes which coupled, *viz.* the fast mode, which changed direction and coupled with the forward propagating slow mode, and the two coupled slow mode waves, respectively, in the model with a single beam and asymmetric counterstreaming beams. The instability (and damping) regimes vanish when the waves decouple for higher beam speeds.

In proceeding to investigate the nonlinear structures, we have identified two beam speed regimes, respectively, low and high for which the dispersion function $F(M)$ (which corresponds to the second derivative of the Sagdeev potential evaluated at $\Phi = 0$) assumes positive or negative values in intermediate regions of wave phase speed M between the two pairs of critical acoustic speeds in which the derivative of the function changes sign. The M ($\equiv \Omega/K$) values for which $F(M) = 0$ coincide with the phase speeds of the linear waves in the limit of small K are the critical acoustic speeds, which, traditionally, are the minimum speeds for soliton existence.

The situation for $F(M)$, which is positive-valued in the interval between the pair of critical acoustic speeds F and G, in which the derivative of the function changes sign from positive to negative, corresponds to two linear waves, which are coupled, and the dispersion curves are double-branched in ω_r/ω_{pe} in ranges of small and large $k\lambda_{de}$. The waves associated with the lower (upper) branch are unstable (stable). This explains the unusual character of the nonlinear structures, which are subsonic (supersonic) in the model with a single electron beam (asymmetric counterstreaming electron beams) as the waves are associated with the lower branch of the dispersion curves and their existence is found to be limited by $V(\Phi, M)$ not being defined for negative values of Φ for small (large) values of M .

The dispersion function $F(M)$ which is negative-valued in the interval between the pair of critical acoustic speeds J and K (or O and P), in which the derivative of the function changes sign from negative to positive for higher beam speeds, corresponds to the situation in which the linear modes have uncoupled signified by the dispersion curves for ω_r/ω_{pe} , which have separated and are distinct for the two modes. The nonlinear structures do not exhibit unusual characteristics

in this high beam speed regime as the waves in the linear regime are now stable.

A key finding in our study is that the subsonic character of the solitons in the nonlinear regime is the result of the directional change of the backward propagating fast mode to the forward direction in the single beam model and the directional changes of both the backward and forward propagating slow modes in the model with asymmetric counterstreaming beams. These insights were then applied to attribute the subsonic character of the two slow mode waves in the model with symmetric counterstreaming beams to the directional changes of these two slow mode waves, which would otherwise be difficult to detect due to the symmetric propagation characteristics of the forward and backward propagating slow electron-acoustic mode waves in this model.

There is consistency across the models in both the low and high beam speed regimes, for which $F(M)$ is negative-valued in the interval between the pair of critical acoustic speeds in which the derivative of the function changes sign. It is found that soliton propagation is continuous in the range in M between the critical acoustic speeds labeled J and K in the plots of $F(M)$ for low values of the speed(s) of the beam(s), however, a stopband region for soliton propagation occurs between the critical acoustic speeds labeled O and P in the plots of $F(M)$ for high beam speeds. The effect of current neutral plasma conditions in equilibrium which is satisfied in our models with symmetric and asymmetric counterstreaming beams but violated in the single beam model, appears to have no significant effect on the overall characteristics of the waves in the nonlinear regime. The main difference is that there is less symmetry breaking in a plasma with asymmetric counterstreaming beams in which model the two slow waves propagate in opposite directions and symmetry is retained even for high beam speeds (there are two forward propagating and two backward propagating waves) in contrast to the model with a single beam (there are three forward propagating and one backward propagating waves).

The results of our study, which are generic, can be applied to explaining the subsonic character of ion-acoustic solitons in studies by Lakhina *et al.*¹⁹ and Zank and McKenzie,²¹ respectively, in models with counterstreaming and single ion beams, and the subsonic character of electron-acoustic solitons in the single electron beam model of Berthomier *et al.*¹³

AUTHOR DECLARATIONS

Conflict of Interest

The authors have no conflicts to disclose.

Author Contributions

S. K. Maharaj: Conceptualization (equal); Formal analysis (equal); Writing – original draft (equal). **R. Bharuthram:** Writing – review & editing (equal).

DATA AVAILABILITY

The data that support the findings of this study are available from the corresponding author upon reasonable request.

REFERENCES

1. S. P. Gary, *Phys. Fluids* **30**, 2745–2749 (1987).

- ²R. Bharuthram, *J. Plasma Phys.* **46**, 1–10 (1991).
- ³L. N. Mbuli, S. K. Maharaj, and R. Bharuthram, *Phys. Plasmas* **20**, 122115 (2013).
- ⁴R. Bharuthram, *Astrophys. Space Sci.* **202**, 337–347 (1993).
- ⁵L. N. Mbuli, S. K. Maharaj, and R. Bharuthram, *Phys. Plasmas* **21**, 052115 (2014).
- ⁶R. L. Mace, S. Baboolal, R. Bharuthram, and M. A. Hellberg, *J. Plasma Phys.* **45**, 323 (1991).
- ⁷R. E. Ergun, C. W. Carlson, J. P. McFadden, F. S. Mozer, G. T. Delory, W. Peria, C. C. Chaston, M. Temerin, I. Roth, L. Muschietti, R. Elphic, R. Strangeway, R. Pfaff, C. A. Cattell, D. Klumpar, E. Shelley, W. Peterson, E. Moebius, and L. Kistler, *Geophys. Res. Lett.* **25**, 2041, <https://doi.org/10.1029/98GL00636> (1998).
- ⁸J. R. Franz, P. M. Kintner, and J. S. Pickett, *Geophys. Res. Lett.* **25**, 1277, <https://doi.org/10.1029/98GL50870> (1998).
- ⁹H. Matsumoto, H. Kojima, T. Miyatake, Y. Omura, M. Okada, I. Nagano, and M. Tsutsui, *Geophys. Res. Lett.* **21**, 2915, <https://doi.org/10.1029/94GL01284> (1994).
- ¹⁰S. D. Bale, P. J. Kellogg, D. E. Larsen, R. P. Lin, K. Goetz, and R. P. Lepping, *Geophys. Res. Lett.* **25**, 2929, <https://doi.org/10.1029/98GL02111> (1998).
- ¹¹J. S. Pickett, J. D. Menietti, D. A. Gurnett, B. Tsurutani, P. M. Kintner, E. Klatt, and A. Balogh, *Nonlinear Processes Geophys.* **10**, 3 (2003).
- ¹²V. L. Krasovsky, H. Matsumoto, and Y. Omura, *J. Geophys. Res.* **102**, 22131, <https://doi.org/10.1029/97JA02033> (1997).
- ¹³M. Berthomier, R. Pottelette, M. Malingre, and Y. Khotyaintsev, *Phys. Plasmas* **7**, 2987–2994 (2000).
- ¹⁴T. Cattaert, F. Verheest, and M. A. Hellberg, *Phys. Plasmas* **12**, 042901 (2005).
- ¹⁵S. K. Maharaj, R. Bharuthram, S. V. Singh, and G. S. Lakhina, *Phys. Plasmas* **19**, 122301 (2012).
- ¹⁶S. V. Singh, G. S. Lakhina, R. Bharuthram, and S. R. Pillay, *Phys. Plasmas* **18**, 122306 (2011).
- ¹⁷L. N. Mbuli, S. K. Maharaj, R. Bharuthram, S. V. Singh, and G. S. Lakhina, *Phys. Plasmas* **22**, 062307 (2015).
- ¹⁸L. N. Mbuli, S. K. Maharaj, R. Bharuthram, S. V. Singh, and G. S. Lakhina, *Phys. Plasmas* **23**, 062302 (2016).
- ¹⁹G. S. Lakhina, S. V. Singh, and R. Rubia, *Phys. Scr.* **95**, 105601 (2020).
- ²⁰F. Verheest and M. A. Hellberg, *Phys. Scr.* **96**, 045643 (2021).
- ²¹G. P. Zank and J. F. McKenzie, *J. Plasma Phys.* **39**, 183–191 (1988).
- ²²K. Singh, S. S. Varghese, F. Verheest, and I. Kourakis, *Astrophys. J.* **957**(14pp), 96 (2023).
- ²³M. Maxengana, S. K. Maharaj, and R. Bharuthram, *Phys. Plasmas* **32**, 082304 (2025).
- ²⁴C. S. Lin, J. L. Burch, S. D. Shawhan, and D. A. Gurnett, *J. Geophys. Res.* **89**, 925–935, <https://doi.org/10.1029/JA089iA02p00925> (1984).
- ²⁵R. D. Sharp, E. G. Shelley, R. G. Johnson, and A. G. Ghielmetti, *J. Geophys. Res.* **85**, 92–100, <https://doi.org/10.1029/JA085iA01p00092> (1980).
- ²⁶C. Chang, K. Huang, Q. Lu, S. Lu, X. Yu, R. Wang, L. Sang, and X. Gao, *Astrophys. J.* **933**, 67 (2022).
- ²⁷S. S. Ghosh, K. K. Ghosh, and A. N. Sekar Iyengar, *Phys. Plasmas* **3**, 3939–3946 (1996).
- ²⁸F. Verheest, M. A. Hellberg, and I. Kourakis, *Phys. Plasmas* **15**, 112309 (2008).
- ²⁹C. P. Olivier, S. K. Maharaj, and R. Bharuthram, *Phys. Plasmas* **23**, 064701 (2016).
- ³⁰C. P. Olivier, S. K. Maharaj, and R. Bharuthram, *Phys. Plasmas* **22**(8), 082312 (2015).
- ³¹Q. Lu, S. Wang, and X. Dou, *Phys. Plasmas* **12**, 072903 (2005).
- ³²C. S. Lin, D. Winske, and R. L. Tokar, *J. Geophys. Res.* **90**, 8269–8280, <https://doi.org/10.1029/JA090iA09p08269> (1985).
- ³³E. J. Koen, A. B. Collier, and S. K. Maharaj, *Phys. Plasmas* **19**, 042101 (2012).
- ³⁴J. B. Tao, R. E. Ergun, D. L. Newman, J. S. Halekas, L. Andersson, V. Angelopoulos, J. W. Bonnell, J. P. McFadden, C. M. Cully, H.-U. Auster, K.-H. Glassmeier, D. E. Larson, W. Baumjohann, and M. V. Goldman, *J. Geophys. Res.* **117**, A03106, <https://doi.org/10.1029/2011ja017364> (2012).
- ³⁵E. Okutsu, M. Nakamura, Y. Nakamura, and T. Itoh, *Plasma Phys.* **20**, 561–568 (1978).
- ³⁶Y. Nakamura and K. Komatsuda, *J. Plasma Phys.* **60**, 69–80 (1998).
- ³⁷Y. Nakamura, H. Bailung, and R. Ichiki, *Phys. Plasmas* **11**, 3795–3800 (2004).